Neuro-Oncology

Neuro-Oncology 18(6), 873–880, 2016
doi:10.1093/neuonc/nov301
Advance Access date 19 December 2015

A prospective trial of dynamic contrast-enhanced MRI perfusion and fluorine-18 FDG PET-CT in differentiating brain tumor progression from radiation injury after cranial irradiation

Vaios Hatzoglou†, T. Jonathan Yang†, Antonio Omuro, Igor Gavrilovic, Gary Ulaner, Jennifer Rubel, Taylor Schneider, Kaitlin M. Woo, Zhigang Zhang, Kyung K. Peck, Kathryn Beal‡, and Robert J. Young‡

Department of Radiology, Neuroradiology Service, Memorial Sloan Kettering Cancer Center, New York, New York (V.H., J.R., T.S., K.K.P., R.J.Y.); Department of Radiation Oncology, Memorial Sloan Kettering Cancer Center, New York, New York (T.J.Y., K.B.); Department of Radiology, Molecular Imaging and Therapy Service, Memorial Sloan Kettering Cancer Center, New York, New York (G.U.); Department of Neurology, Memorial Sloan Kettering Cancer Center, New York, New York (A.O., I.G.); Department of Epidemiology and Biostatistics, Memorial Sloan Kettering Cancer Center, New York, New York (K.M.W., Z.Z.); Department of Medical Physics, Memorial Sloan Kettering Cancer Center, New York, New York (K.K.P.); Brain Tumor Center, Memorial Sloan Kettering Cancer Center, New York, New York (V.H., A.O., I.G., K.B., R.J.Y.)

Corresponding Author: Robert J. Young, MD, Department of Radiology, Memorial Sloan Kettering Cancer Center, 1275 York Avenue, New York, NY 10065 (youngr@mskcc.org).

†V.H. and T.J.Y. contributed equally to this work as co-first authors.

‡K.B. and R.J.Y. contributed equally to this work as co-senior authors.

Background. The aim of this study was to assess the effectiveness of fluorine-18 fluorodeoxyglucose (FDG) PET-CT and dynamic contrast-enhanced (DCE) MRI in differentiating tumor progression and radiation injury in patients with indeterminate enhancing lesions after radiation therapy (RT) for brain malignancies.

Methods. Patients with indeterminate enhancing brain lesions on conventional MRI after RT underwent brain DCE-MRI and PET-CT in a prospective trial. Informed consent was obtained. Lesion outcomes were determined by histopathology and/or clinical and imaging follow-up. Metrics obtained included plasma volume (Vp) and volume transfer coefficient (K^{trans}) from DCE-MRI, and maximum standardized uptake value (SUV_{max}) from PET-CT; lesion-to-normal brain ratios of all metrics were calculated. The Wilcoxon rank sum test and receiver operating characteristic analysis were performed.

Results. The study included 53 patients (29 treated for 29 gliomas and 24 treated for 26 brain metastases). Progression was determined in 38/55 (69%) indeterminate lesions and radiation injury in 17 (31%). Vp_{ratio} ($V_{P\ lesion}/V_{P\ normal\ brain}$, $P < .001$), K^{trans}_{ratio} ($P = .002$), and SUV_{ratio} ($P = .002$) correlated significantly with diagnosis of progression versus radiation injury. Progressing lesions exhibited higher values of all 3 metrics compared with radiation injury. Vp_{ratio} had the highest accuracy in determining progression (area under the curve = 0.87), with 92% sensitivity and 77% specificity using the optimal, retrospectively determined threshold of 2.1. When Vp_{ratio} was combined with K^{trans}_{ratio} (optimal threshold 3.6), accuracy increased to 94%.

Conclusions. Vp_{ratio} was the most effective metric for distinguishing progression from radiation injury. Adding K^{trans}_{ratio} to Vp_{ratio} further improved accuracy. DCE-MRI is an effective imaging technique for evaluating nonspecific enhancing intracranial lesions after RT.

Keywords: DCE MRI perfusion, 18F-FDG PET-CT, radiation injury.

Radiation therapy (RT) has an essential role in providing local control and prolonging survival of patients with intracranial primary malignancies (gliomas) as well as those with brain metastases.[1–4] While RT is effective in disease control, it often results in radiation injury at treatment sites, which may manifest months to years later.[5] In patients treated for gliomas with

Received 2 August 2015; accepted 6 November 2015

standard fractionated RT and systemic therapy, the radiation injury rate has been reported to be 5%–10%.[6] In the treatment of metastasis using single-fraction stereotactic radiosurgery (SRS), radiation injury rates may reach 18% or greater.[7,8]

Conventional MRI is often unable to reliably distinguish between progression and radiation injury, as both may manifest with new and/or growing enhancing lesions.[9,10] For patients with indeterminate findings on conventional MRI, treatment decision making is difficult, as progression usually demands a significant change in therapeutic approach to ensure tumor control.[11,12] Although some patients (25% in the series reported upon here) do undergo surgical resection of enhancing lesions for neurologic symptom management and improvement of long-term outcome, allowing for definitive histopathologic diagnosis, resection is a risky invasive procedure and may not be suitable for all patients, especially those with multiple lesions, lesions in inaccessible locations, or progressive extracranial disease.[13,14] In addition, histopathology is susceptible to sampling error. Therefore, an accurate, non-invasive imaging technique for diagnosing progression or radiation injury is needed.

Biologically, progression and radiation injury represent 2 different mechanistic processes: tumor progression causes increased enhancement due to tumor-induced angiogenesis and microvascular proliferation,[15] while RT causes increased enhancement by inducing small-vessel endothelial damage and reducing microvasculature.[16,17] Due to this fundamental pathophysiologic difference, advanced imaging modalities such as dynamic contrast-enhanced (DCE) MRI and fluorine-18 fluorodeoxyglucose (FDG) PET-CT have been advocated for the assessment of indeterminate enhancing lesions after RT. DCE-MRI correlates with microvascular density at angiography and histopathology[18] and can quantify the inflammatory and vascular endothelial growth factor–mediated vascular changes that occur with tumor progression and radiation injury.[19,20] FDG PET-CT has been shown to be useful in differentiating progression and radiation injury through metabolic differences, with higher uptake in active tumor cells.[21] DCE-MRI and FDG PET-CT are commonly performed for the diagnosis of progression and radiation injury in patients with enhancing lesions of indeterminate etiology after RT, but their comparative predictive value, sensitivity, and specificity remain uncertain. In this study, we prospectively evaluated the efficacy of DCE-MRI and FDG PET-CT in predicting whether new or worsening enhancing brain lesions seen after RT represented progression or radiation injury.

Materials and Methods

Patient Selection

This prospective trial was approved by the local institutional review board and privacy board (ClinicalTrials.gov # NCT01604512). Written informed consent was obtained from all patients. The inclusion criteria were age ≥18 years, pathological or clinical/radiological diagnosis of a primary or secondary brain tumor, completion of RT, and new and/or increasing enhancing brain lesion(s) at the treated site considered indeterminate for progression versus radiation injury by the neuroradiologist and clinician. The exclusion criterion was a contraindication to PET-CT or MRI scan or gadolinium contrast. Fifty-three patients (35 male and 18 female) with 55 indeterminate lesions and mean and median age of 57 years (range, 19–81) were enrolled.

DCE-MRI and PET-CT examinations were performed ≤12 weeks from the diagnosis of the indeterminate lesion and ≤12 weeks of each other, with either the DCE-MRI or the PET-CT acquired first. The accrual period for this study was from June 2012 through January 2014.

Dynamic Contrast-Enhanced MRI Acquisition and Analysis

Patients were scanned on 1.5T or 3T scanners (Signa HDxt/Excite, Discovery 450/750, GE Healthcare) using an 8-channel head coil. Images acquired in multiple planes were standard T1-weighted (repetition time/echo time [TR/TE], 525/7 ms for 1.5T; 1800/7 ms for 3T), T2-weighted (TR/TE, 4000/102 ms for 1.5T; 3100/101 ms for 3T), diffusion-weighted (TR/TE, 8000/85 ms for 1.5T and 3T), fluid-attenuated inversion recovery (TR/TE, 8000/160 ms for 1.5T; TR/TE, 9000/120 ms for 3T), susceptibility-weighted (TR/TE, 5000/25 ms for 1.5T; 38/23 ms for 3T), and contrast T1-weighted (TR/TE, 560/8 ms for 1.5T; 1842/7 ms for 3T).

T1-weighted DCE perfusion data were acquired using an axial 3D echo-spoiled gradient-echo sequence: TR, 4–5 ms; TE, 1–2 ms; flip angle, 25 degrees; slice thickness, 5 mm; field of view, 24 cm. Ten to 14 slices were acquired to cover the entire lesion volume. The time between phases (temporal resolution) was 5–6 sec per volume with 40 phases, 10 before and 30 immediately after i.v. bolus administration of a single dose of contrast material (0.2 mL/kg to maximum 20 mL gadopentetate dimeglumine; Bayer HealthCare Pharmaceuticals), total scan time 3 min 20 sec to 4 min. Axial contrast T1-weighted images were also obtained to match the DCE images. The raw data were transferred to an offline image processing workstation.

A board-certified neuroradiologist with 8 years of neuroimaging experience processed the DCE-MRI data in nordicICE (NordicNeuroLab). Using a 2-compartment model with kinetic modeling and arterial input function–based vascular deconvolution as proposed by Murase,[22] maps were calculated of plasma volume (Vp), extravascular extracellular distribution volume (Ve), volume transfer coefficient between plasma and extravascular extracellular space (K^{trans} = distribution into tissue; Kep = distribution away from tissue), and area under the perfusion time curve (AUPC). Each map was overlaid onto the matching contrast T1-weighted image, and DCE analysis was performed by placing 3–5 small fixed-diameter (50–75 mm^2) regions of interest (ROIs) targeted to the most visually apparent abnormalities in the lesion on each perfusion color map. This method of analysis has been described as providing the most accurate and reproducible results.[23–25] Areas of hemorrhage, calcification, cystic/necrotic change, and vessels were explicitly excluded by careful review of all available MRI sequences for each case, particularly the susceptibility-weighted imaging and pre-contrast T1 images.

For each individual perfusion color map, the most abnormally elevated of the 3–5 measurements was selected and then normalized by placing a fixed-diameter (50–75 mm^2) ROI in

the normal contralateral white matter and calculating the ratio of the lesion measurement to the normal white matter measurement; the ratios (hereafter referred to as Vp_{ratio}, Ve_{ratio}, K^{trans}_{ratio}, Kep_{ratio}, and $AUPC_{ratio}$) were recorded for analysis.

Fluorodeoxyglucose PET-CT Protocol and Analysis

Ten millicuries of fluorine-18 FDG was i.v. injected, with the patient remaining seated in the injection room for 60 min. The patient was then positioned on a PET-CT scanner (Discovery STE, GE Healthcare). A spiral CT was acquired using a full helical acquisition at 1 sec/rotation, 30 mA, 140 kV; slice thickness, 5 mm. Immediately upon completion of the CT, a 10-min 3D PET scan was acquired. CT and PET data were reconstructed using a 30-cm field of view. A radiologist board certified in radiology and nuclear medicine with 9 years of PET-CT experience defined ROIs for the lesion and normal brain. The maximum standardized uptake value (SUV_{max}) of the lesion and normal brain were measured. The brain FDG PET-CT was windowed to visualize the focal FDG avidity associated with the known brain lesion on MRI, then an ROI was placed to encompass the entire area of abnormal FDG avidity. SUV_{max} was measured from the voxel with the highest SUV within this ROI. Calculation of lesional SUV_{max} was reproducible, as the voxel with the highest SUV was consistently within a range of possible ROIs. A second ROI was then drawn in comparable contralateral normal brain to measure SUV_{max} for normal brain background. The ratio of lesion SUV_{max} and normal brain SUV_{max} (SUV_{ratio}) was then calculated and used for further analysis.

Lesion Diagnosis

When available, histopathology after resection of the indeterminate enhancing lesion was used to determine diagnosis. Progression was determined by the presence of any amount of tumor in the resected lesion. Radiation injury was determined by the complete absence of any identifiable tumor. For patients with nonhistopathologic diagnoses, determination of progression or radiation injury was made using modified criteria from the RANO (Response Assessment in Neuro-Oncology) working group.[26] Progression was determined by continued increase in size of the enhancing lesion (≥25% in sum of product of perpendicular diameters) or if the patient experienced progressive clinical worsening of neurologic function requiring salvage therapy. Radiation injury was determined by the absence of clinical worsening and the spontaneous stabilization or decrease of the enhancing lesion on subsequent MRI scans for a minimum of 6 months without new therapy.[27] Lesion diagnosis was made by an experienced radiation oncologist blinded to the DCE-MRI and PET-CT data.

Statistical Analysis

Clinical characteristics were compared between patients with gliomas and patients with metastases using Fisher's test and the Wilcoxon rank sum test. The Wilcoxon rank sum test was also used to determine the significance of correlations between DCE-MRI and PET-CT imaging metrics (Vp_{ratio}, Ve_{ratio}, K^{trans}_{ratio}, Kep_{ratio}, $AUPC_{ratio}$, and SUV_{ratio}) and progression versus radiation injury. After Bonferroni adjustment for multiple testing, the P-value was set to $<.007$ ($P < .05$ divided by 7 tests). Receiver operating characteristics analysis was performed for the imaging metrics found to be significant on the Wilcoxon rank sum test, and the area under the curve (AUC) was computed. Threshold values for the different imaging metrics were estimated by maximizing the sum of sensitivity and specificity. Subgroup analyses were also performed for the gliomas and the metastases.

Results

Patient Characteristics

Twenty-nine patients received RT for 29 gliomas, and the majority of these (97%) were treated with postoperative partial-brain RT (PBRT) to a median dose of 60 Gy (range, 26–60 Gy). Twenty-four patients received RT for 26 brain metastases; the treatments consisted of definitive SRS (42% of metastases; median dose, 21 Gy; range, 15–21 Gy), postoperative PBRT (12%; median dose, 30 Gy; range, 30–36 Gy), and various combinations of SRS, PBRT, and whole-brain RT (Table 1).

The median time between RT and detection of the indeterminate lesion was 9 months (range, 1–99 mo), with no significant difference between the glioma group (median, 9 mo; range, 1–99 mo) and the metastasis group (median, 10 mo; range, 3–40 mo; $P = .83$). The median time between detection of lesions in question and the first protocol scan was 1 month (range, 0–2.8 mo). The median time between the protocol DCE-MRI and FDG PET-CT scans was 1 day (range, 0–84 d), with 36 patients (68%) completing the scans within 7 days; 41 patients (77%) completing them within 14 days; and 48 patients (91%) completing them within 30 days.

Clinical Outcomes Determination

Of the 55 indeterminate enhancing lesions assessed in the study, 38 (69%) were determined to be progression and 17 (31%) were determined to be radiation injury through either histopathologic examination after surgical resection ($n = 14$, 25%) or longitudinal clinical and radiological evaluation ($n = 41$ lesions, 75%). Progression was diagnosed more frequently for gliomas (93%) than for brain metastases (42%, $P < .001$, Table 1). The proportion of patients diagnosed with progression through surgical pathology did not differ significantly between the glioma cohort (23%) and the brain metastases cohort (28%, $P = .76$). At time of progression, patients with glioma were being treated with temozolomide ($n = 7$), bevacizumab ($n = 6$), 2 BKM120 ($n = 2$), carmustine ($n = 1$), carboplatin ($n = 1$), or irinotecan ($n = 1$). At time of progression, patients with metastases were being treated with bevacizumab ($n = 2$).

Correlation Between Dynamic Contrast-Enhanced MRI/PET-CT Metrics and Clinical Outcomes

As summarized in Table 2, increased Vp_{ratio} ($P < .001$) and K^{trans}_{ratio} ($P = .002$) were significantly associated with progression, while Kep_{ratio}, Ve_{ratio}, and $AUPC_{ratio}$ were not ($P > .17$). Optimal threshold values were retrospectively determined from the data. When a Vp_{ratio} threshold of ≥2.1 was used to declare progression, sensitivity was 92% (ie, 35 of 38 lesions representing

Table 1. Patient characteristics

Characteristics	All Patients, $n = 53$	Patients with Gliomas, $n = 29$	Patients with Brain Metastases, $n = 24$	P
Lesions (%)	55	29 (52.7)	26 (47.3)	
Median age, y (range)	57 (19–81)	53 (19–72)	63 (24–81)	.13
Histology				
Astrocytoma*				
IV	18 (33)	18 (62)		
III	6 (11)	6 (21)		
II	2 (4)	2 (7)		
Oligodendroglioma*				
III	2 (4)	2 (7)		
II	1 (2)	1 (3)		
Metastasis				
NSCLC	7 (13)		7 (27)	
Breast	7 (13)		7 (27)	
Melanoma	5 (9)		5 (19)	
Other	7 (13)		7 (27)	
Type of radiation therapy				
PBRT only	31 (56)	28 (97)	3 (12)	
SRS only	11 (20)		11 (42)	
PBRT + WBRT	3 (5)		2 (8)	
SRS + WBRT	8 (15)		8 (31)	
SRS + PBRT	2 (4)	1 (3)	2 (8)	
Clinical outcome				<.001
Tumor progression	38 (69)	27 (93)	11 (42)	
Radiation injury	17 (31)	2 (7)	15 (58)	

Abbreviations: NSCLC, non-small cell lung cancer; WBRT, whole-brain RT.
*World Health Organization grade.

Table 2. DCE-MRI and PET-CT imaging metrics used to determine accuracy in predicting disease progression vs radiation injury

Variables	Disease Progression			Radiation Injury			P^a	AUC
	Mean	Range	SE	Mean	Range	SE		
DCE-MRI								
Vp_{ratio}	6.2	1.5–41.9	1.3	2.1	1.1–7.8	0.4	<.001	0.87
K^{trans}_{ratio}	31.8	0.4–363	10.9	6.3	0.3–28.4	2.1	.002	0.76
$K21_{ratio}$	91.8	1.0–700	24.6	54.7	0.7–250	19.6	.21	0.61
Ve_{ratio}	928	3.6–17 360	616	1068	1.4–12 275	770	.17	0.62
$AUPC_{ratio}$	7.9	1.3–47.3	1.5	9.5	1.2–39.0	2.9	.18	0.62
PET-CT								
SUV_{ratio}	1.6	1.0–4.2	0.1	1.1	1.0–1.9	0.1	.002	0.75

[a]Wilcoxon rank sum test.

progression were correctly classified as progression) and specificity was 77% (the rate of correct classification of radiation injury as radiation injury). The use of a K^{trans}_{ratio} threshold of $\geq$3.6 to declare progression yielded sensitivity of 87% and specificity of 71%. The PET-CT SUV_{ratio} was also a significant predictor of progression ($P = .002$). The use of an SUV_{ratio} threshold of $\geq$1.2 to declare progression yielded sensitivity of 68% and specificity of 82% (Fig. 1). Representative cases are shown in Figs 2 and 3.

Of the 38 lesions determined to be progression, 3 (8%) did not reach the Vp_{ratio} optimal threshold of 2.1, five (13%) did not reach the K^{trans}_{ratio} threshold of 3.6, and 12 (32%) did not reach the SUV_{ratio} threshold of 1.2. Of the 3 progressing lesions below threshold for Vp_{ratio}, 2 were also below threshold for K^{trans}_{ratio} and all 3 were below threshold for SUV_{ratio}. Of the 17 lesions determined to be radiation injury, 3 (18%) had an $SUV_{ratio} > 1.2$, four (24%) had a $Vp_{ratio} > 2.1$, and 5 (29%)

had a $K^{trans}_{ratio} > 3.6$. Of the 3 radiation injury lesions above threshold for SUV_{ratio}, 2 were also above threshold for Vp_{ratio}, and 2 were above threshold for K^{trans}_{ratio}.

Discordance Between Predictions Made with DCE-MRI and PET-CT Metrics

When utilizing $Vp_{ratio} \geq 2.1$ and $SUV_{ratio} \geq 1.2$ as thresholds for predicting tumor progression, the results were discordant for 12 lesions. Vp_{ratio} correctly predicted tumor in 9 of these lesions (MR perfusion [MRP] and PET were performed on the same day for 4 lesions; PET preceded MRP for 4 lesions by 83, 34, 25, and 18 days; MRP preceded PET for 1 lesion by 1 day). There were no discordant cases of PET-CT correctly predicting tumor progression when Vp_{ratio} did not meet the threshold of 2.1. Vp_{ratio} correctly predicted radiation injury for 1 lesion that demonstrated an $SUV_{ratio} \geq 1.2$ ($SUV_{ratio} = 1.7$; MRP and PET performed on the same day). PET-CT correctly predicted radiation injury in 2 lesions for which Vp_{ratio} predicted tumor progression ($Vp_{ratio} = 7.77$ and 2.52; both lesions in the same patient, MRP preceded PET by 18 days).

When a $K^{trans}_{ratio} \geq 3.6$ and an $SUV_{ratio} \geq 1.2$ were used as optimal thresholds for predicting tumor progression, the results were discordant for 18 lesions. K^{trans}_{ratio} correctly predicted tumor in 10 of these lesions (MRP and PET were performed on the same day for 5 lesions; PET preceded MRP for 4 lesions by 83, 34, 25, and 18 days; MRP preceded PET for 1 lesion by 1 day). K^{trans}_{ratio} correctly predicted radiation injury in 1 lesion that was predicted to be tumor by PET-CT ($SUV_{ratio} = 1.9$; PET preceded MRP by 1 day). PET-CT correctly predicted tumor progression in 4 lesions for which K^{trans}_{ratio} predicted radiation injury (MRP and PET were performed on the same day for 2 lesions; MRP preceded PET for 2 lesions by 2 and 7 days). PET-CT correctly predicted radiation injury in 3 lesions for which K^{trans}_{ratio} predicted tumor progression (MRP and PET were performed on the same day for 2 lesions; PET preceded MRP for 1 lesion by 10 days).

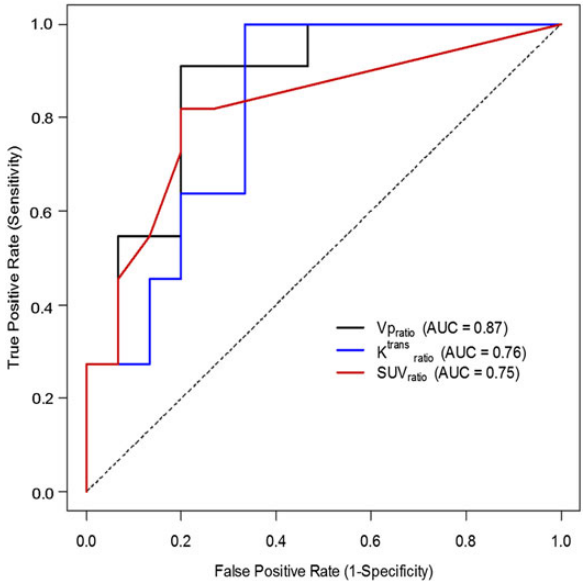

Fig. 1. Receiver operating characteristic (ROC) analysis for Vp_{ratio}, K^{trans}_{ratio}, and SUV_{ratio} demonstrating the optimal cutoffs to be 2.1, 3.6, and 1.2, respectively, in distinguishing between progression and radiation injury.

Correlation of Combinations of DCE-MRI and PET-CT Metrics with Clinical Outcomes

We next explored combinations of DCE-MRI and PET-CT metrics to determine whether they would further improve prediction of clinical outcomes. When using the optimal thresholds of $Vp_{ratio} \geq 2.1$ and $K^{trans}_{ratio} \geq 3.6$, the combination of these 2 metrics had sensitivity of 79% for accurate diagnosis of progression, and specificity of 94% for accurate diagnosis of radiation injury. Compared with using Vp_{ratio} alone, combining Vp_{ratio} and K^{trans}_{ratio} improved accuracy in predicting radiation injury but not progression. When $Vp_{ratio} \geq 2.1$ and $SUV_{ratio} \geq 1.2$ were combined, the rate of correct classification of progression was 66% and

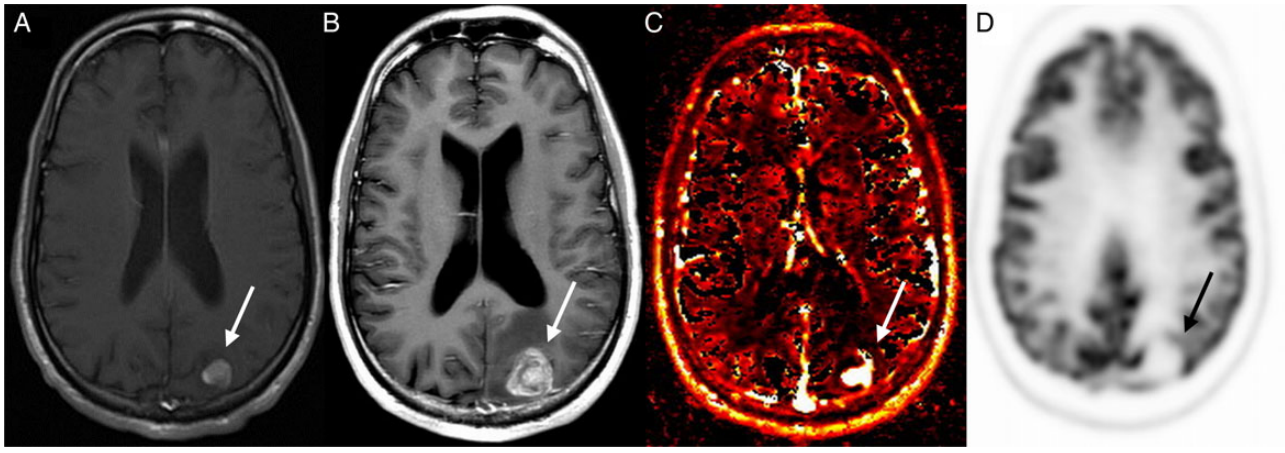

Fig. 2. Patient example of tumor progression detected by DCE-MRI perfusion. Images obtained in a 30-year-old man with metastatic sarcoma who underwent SRS to a left parietal lobe metastasis. Axial contrast-enhanced T1-weighted image before treatment (A) shows an enhancing mass (arrow) that increases in size 6 months after treatment (B). Vp map of the enlarging mass (C) demonstrates increased perfusion; however, PET-CT showed no abnormal FDG uptake (D). Pathology confirmed progression.

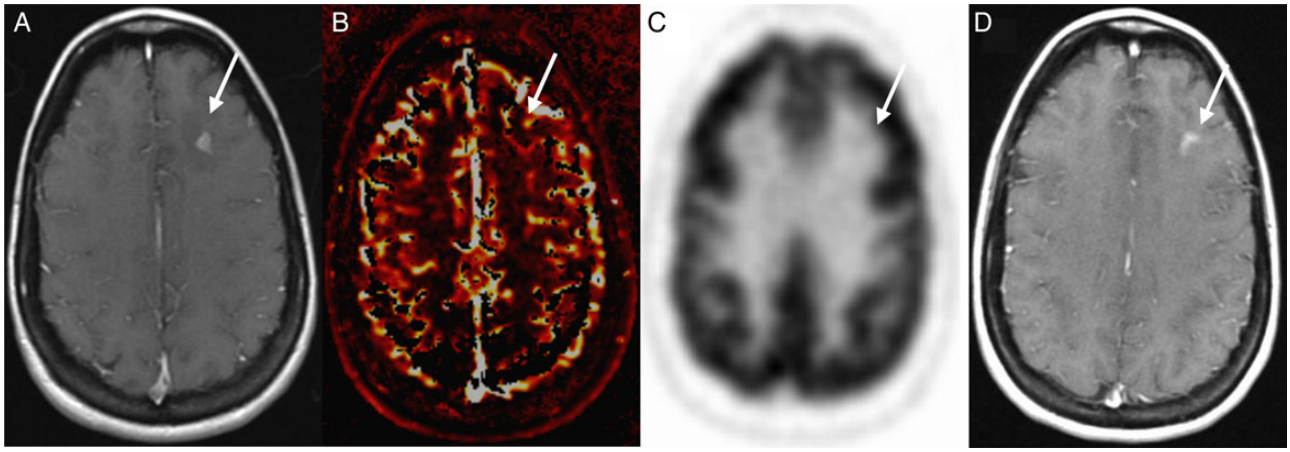

Fig. 3. Patient example of radiation injury detected by DCE-MRI perfusion and PET-CT. Images obtained in a 39-year-old woman with metastatic breast cancer who underwent SRS to a left frontal lobe metastasis. Axial contrast-enhanced T1-weighted image (A) demonstrates an enhancing mass that had increased in size 1 year after SRS (arrow). DCE-MRI showed no increase in perfusion on the Vp map (B) and no increase in SUV on PET-CT (C). The lesion remained stable 1 year after it had enlarged (D) without any additional therapy and was determined to represent radiation injury.

the rate of correct classification of radiation injury was 88%, also improving the predictive value for radiation injury compared with any individual metric.

Subgroup Analyses

The metastasis subgroup ($n = 26$) consisted of more patients with diagnoses of radiation injury ($n = 15$, 68%) than of progression ($n = 11$, 42%). In this subgroup, Vp_{ratio} remained a significant predictor of radiation injury ($P = .001$), as did K^{trans}_{ratio} ($P = .005$) and SUV_{ratio} ($P = .004$), while the other metrics were not ($P \geq .18$). When a Vp_{ratio} threshold of ≥ 2.6 was used to declare progression, sensitivity was 91% and specificity was 80%. The use of a K^{trans}_{ratio} threshold of ≥ 4.1 to declare progression yielded sensitivity of 100% and specificity of 67%. Vp_{ratio} and K^{trans}_{ratio} measurements were not significantly different between the progressive metastases ($n = 11$) and the progressive gliomas ($n = 27$) ($P = .062$). The use of an SUV_{ratio} threshold of ≥ 1.4 to declare progression yielded sensitivity of 82% and specificity of 80%.

Discussion

DCE-MRI and FDG PET-CT are frequently utilized for the purpose of distinguishing between tumor progression and radiation injury in the brain.[19,20,28–30] However, there is no clear consensus on which modality is more accurate or whether the 2 modalities provide complementary information. In this prospective study, we systematically analyzed the accuracy of DCE-MRI and FDG PET-CT in differentiating progression and radiation injury in patients who developed indeterminate enhancing lesions after RT for gliomas or brain metastases. To our knowledge, this is the largest prospective series providing a direct comparison of the effectiveness of DCE-MRI and FDG PET-CT in the same set of patients. We found that DCE-MRI and PET-CT were both useful in distinguishing between progression and radiation injury, although DCE-MRI (AUC = 0.76–0.87) slightly outperformed PET-CT (AUC = 0.75). The predictive values of these techniques increased when they were used in combination.

Compared with conventional MRI alone, DCE-MRI can improve diagnosis, predict prognosis, and inform treatment decisions in patients with brain tumors.[31,32] While the literature has demonstrated the benefits of using DCE-MRI in distinguishing progression and radiation injury, the majority of the studies were retrospective and included small numbers of patients. Metrics such as increased cerebral blood volume ratio,[20,33] decreased percentage of signal-intensity recovery,[20,30] and increased relative peak height[20] have all been associated with progression in both gliomas and brain metastases. A recent study of 33 patients treated with RT for gliomas found that increased K^{trans} and Ve correlated with progression.[34] We did not find Ve to be a significant predictor ($P = .17$), possibly because of heterogeneous contributions to Ve from additional physiologic factors such as capillary bed perfusion and permeability.[35] However, we did find that Vp_{ratio}, which provides estimates of vascular perfusion and microvascular density, and K^{trans}_{ratio}, which provides estimates of vascular leakiness related to altered permeability, permeability surface area product, and flow, were significant predictors. Specifically, Vp_{ratio} was the most robust predictor of progression (AUC = 0.87; 92% sensitivity using a cutoff of 2.1) of the 5 DCE-MRI metrics tested. When Vp_{ratio} and K^{trans}_{ratio} were combined, accuracy in predicting radiation injury improved to 94% from 77% for Vp_{ratio} only and 71% for K^{trans}_{ratio} only. The increased accuracy reflects the complementary roles of Vp_{ratio} and K^{trans}_{ratio}, which investigate different pathophysiologic properties and have been recognized as independent imaging biomarkers.[36,37] We did not detect a difference in Vp_{ratio}, K^{trans}_{ratio}, or SUV_{ratio} between the progressive metastasis subgroup and the progressive glioma subgroup ($P = .062$). We also found similar optimal thresholds for the whole group and the metastasis subgroup; for simplicity, we therefore suggest that the proposed whole-group thresholds are sufficient for routine clinical use regardless of the underlying tumor pathology.

Using FDG PET-CT, we determined that SUV_{ratio} was effective in distinguishing between progression and radiation injury but trended toward lower predictive value compared with Vp_{ratio}

(AUC = 0.75 vs 0.87, $P = .061$). Prior studies have also shown increased SUV_{ratio} in progression[30,38] without finding PET-CT to be superior to DCE-MRI. The combination of Vp_{ratio} with SUV_{ratio} did not yield higher predictive value than Vp_{ratio} alone. The SUV_{ratio} threshold of $\geq$1.2 demonstrated higher specificity for progression than either Vp_{ratio} or K^{trans}_{ratio} alone, but its specificity was lower than that of the combination of Vp_{ratio} and K^{trans}_{ratio} (82% vs 94%). DCE-MRI also performed better than PET-CT when the results of DCE-MRI and PET-CT were discordant. This has implications for clinical care, as DCE-MRI alone may be sufficient for the evaluation of indeterminate lesions in many patients. Furthermore, DCE-MRI may offer the added benefits of being less expensive and less time-consuming than PET-CT, as at some institutions (including ours) patients with brain tumors are already routinely followed with MRI.

Our study had several potential limitations. First, we included a heterogeneous group of patients who had both primary and metastatic tumors. It is possible that optimal cutoff values for distinguishing radiation injury from progression differ between patients with gliomas and patients with metastases, although our results and other studies have shown that they have similar values.[39,40] The inclusion of both primary and metastatic tumors reflects actual practice with heterogeneous patient populations and therefore broadens the potential applicability of our results. Nevertheless, an ongoing subsequent study with a larger patient cohort is under way at our institution, which will allow for more detailed analyses of patients with primary versus metastatic disease. Second, not all patients underwent surgery for their enlarging brain lesions; however, the clinical and radiological criteria we used to determine follow-up outcomes were familiar and commonly applied in research trials and in daily practice. Third, a disproportionate number of the patients with primary tumors were determined to have progression. This may reflect our relatively conservative definitions of radiation injury as complete absence of any tumor at histopathology and no new treatment for a minimum of 6 months at follow-up. Fourth, we were unable to perform subgroup analyses for the glioma cohort due to the unequal numbers of patients in the progression and radiation injury groups. Nevertheless, a subgroup analysis including only the patients treated for brain metastases showed that Vp_{ratio} remained the most effective imaging metric in distinguishing progression and radiation injury. Fifth, the DCE acquisition time may not have been sufficiently long enough to allow for precise measurement of Kep and Ve. We typically observe a new slightly elevated baseline toward the end of the signal-intensity time curve, suggesting that the equilibrium phase has been reached and washout has been achieved. Although extending the time of DCE acquisition would help confirm that equilibrium has been reached, it has been suggested that proper modeling of the tracer kinetics is sufficient to correctly estimate the constancy of the parameters over time.[41–43]

In conclusion, we found that the DCE-MRI metrics Vp_{ratio} and K^{trans}_{ratio}, as well as the SUV_{ratio} derived from FDG PET-CT, were useful in distinguishing progression from radiation injury. Of all the individual metrics assessed, Vp_{ratio} was the most robust predictor of progression, and the combination of Vp_{ratio} and K^{trans}_{ratio} was able to predict radiation injury with 94% accuracy. Our results should be validated in a larger cohort that allows for separate analyses for patients with gliomas and patients with metastases.

Funding

R.J.Y.'s research is partly supported by the Department of Radiology, Memorial Sloan Kettering Cancer Center. K.M.W. and Z.Z.'s research is partly supported by NIH grant P30 CA008748.

Acknowledgments

The authors are grateful for the expert editorial advice given by Ada Muellner, Department of Radiology, Memorial Sloan Kettering Cancer Center.

Conflict of interest statement. None declared.

References

1. Stupp R, Mason WP, van den Bent MJ, et al. Radiotherapy plus concomitant and adjuvant temozolomide for glioblastoma. *N Engl J Med*. 2005;352(10):987–996.
2. Stupp R, Hegi ME, Mason WP, et al. Effects of radiotherapy with concomitant and adjuvant temozolomide versus radiotherapy alone on survival in glioblastoma in a randomised phase III study: 5-year analysis of the EORTC-NCIC trial. *Lancet Oncol*. 2009;10(5):459–466.
3. Patchell RA, Tibbs PA, Regine WF, et al. Postoperative radiotherapy in the treatment of single metastases to the brain: a randomized trial. *JAMA*. 1998;280(17):1485–1489.
4. Kocher M, Soffietti R, Abacioglu U, et al. Adjuvant whole-brain radiotherapy versus observation after radiosurgery or surgical resection of one to three cerebral metastases: results of the EORTC 22952-26001 study. *J Clin Oncol*. 2011;29(2):134–141.
5. Dropcho EJ. Neurotoxicity of radiation therapy. *Neurol Clin*. 2010; 28(1):217–234.
6. Ruben JD, Dally M, Bailey M, et al. Cerebral radiation necrosis: incidence, outcomes, and risk factors with emphasis on radiation parameters and chemotherapy. *Int J Radiat Oncol Biol Phys*. 2006;65(2):499–508.
7. Minniti G, Clarke E, Lanzetta G, et al. Stereotactic radiosurgery for brain metastases: analysis of outcome and risk of brain radionecrosis. *Radiat Oncol*. 2011;6:48.
8. Brennan C, Yang TJ, Hilden P, et al. A phase 2 trial of stereotactic radiosurgery boost after surgical resection for brain metastases. *Int J Radiat Oncol Biol Phys*. 2014;88(1):130–136.
9. de Wit MC, de Bruin HG, Eijkenboom W, et al. Immediate post-radiotherapy changes in malignant glioma can mimic tumor progression. *Neurology*. 2004;63(3):535–537.
10. Mullins ME, Barest GD, Schaefer PW, et al. Radiation necrosis versus glioma recurrence: conventional MR imaging clues to diagnosis. *.AJNR Am J Neuroradiol*. 2005;26(8):1967–1972.
11. Field KM, Simes J, Nowak AK, et al. Randomized phase 2 study of carboplatin and bevacizumab in recurrent glioblastoma. *Neuro Oncol*. 2015;17(11):1504–1513.
12. Rahmathulla G, Marko NF, Weil RJ. Cerebral radiation necrosis: a review of the pathobiology, diagnosis and management considerations. *J Clin Neurosci*. 2013;20(4):485–502.
13. Field M, Witham TF, Flickinger JC, et al. Comprehensive assessment of hemorrhage risks and outcomes after stereotactic brain biopsy. *J Neurosurg*. 2001;94(4):545–551.

14. Kreth FW, Muacevic A, Medele R, et al. The risk of haemorrhage after image guided stereotactic biopsy of intra-axial brain tumours—a prospective study. *Acta Neurochirurgica*. 2001; 143(6):539–545; discussion 545–546.
15. Gijtenbeek JM, Wesseling P, Maass C, et al. Three-dimensional reconstruction of tumor microvasculature: simultaneous visualization of multiple components in paraffin-embedded tissue. *Angiogenesis*. 2005;8(4):297–305.
16. Remler MP, Marcussen WH, Tiller-Borsich J. The late effects of radiation on the blood brain barrier. *Int J Radiat Oncol Biol Phys*. 1986;12(11):1965–1969.
17. Kamiryo T, Lopes MB, Kassell NF, et al. Radiosurgery-induced microvascular alterations precede necrosis of the brain neuropil. *Neurosurgery*. 2001;49(2):409–414; discussion 414–415.
18. Cha S, Johnson G, Wadghiri YZ, et al. Dynamic, contrast-enhanced perfusion MRI in mouse gliomas: correlation with histopathology. *Magn Reson Med*. 2003;49(5):848–855.
19. Barajas RF Jr., Chang JS, Segal MR, et al. Differentiation of recurrent glioblastoma multiforme from radiation necrosis after external beam radiation therapy with dynamic susceptibility-weighted contrast-enhanced perfusion MR imaging. *Radiology*. 2009; 253(2):486–496.
20. Barajas RF, Chang JS, Sneed PK, et al. Distinguishing recurrent intra-axial metastatic tumor from radiation necrosis following gamma knife radiosurgery using dynamic susceptibility-weighted contrast-enhanced perfusion MR imaging. *.AJNR Am J Neuroradiol*. 2009;30(2):367–372.
21. Chao ST, Suh JH, Raja S, et al. The sensitivity and specificity of FDG PET in distinguishing recurrent brain tumor from radionecrosis in patients treated with stereotactic radiosurgery. *Int J Cancer*. 2001;96(3):191–197.
22. Murase K. Efficient method for calculating kinetic parameters using T1-weighted dynamic contrast-enhanced magnetic resonance imaging. *Magn Reson Med*. 2004;51(4):858–862.
23. Wetzel SG, Cha S, Johnson G, et al. Relative cerebral blood volume measurements in intracranial mass lesions: interobserver and intraobserver reproducibility study. *Radiology*. 2002;224(3):797–803.
24. Young R, Babb J, Law M, et al. Comparison of region-of-interest analysis with three different histogram analysis methods in the determination of perfusion metrics in patients with brain gliomas. *J Magn Reson Imaging*. 2007;26(4):1053–1063.
25. Cha S, Knopp EA, Johnson G, et al. Intracranial mass lesions: dynamic contrast-enhanced susceptibility-weighted echo-planar perfusion MR imaging. *Radiology*. 2002;223(1):11–29.
26. Wen PY, Macdonald DR, Reardon DA, et al. Updated response assessment criteria for high-grade gliomas: Response Assessment in Neuro-Oncology working group. *J Clin Oncol*. 2010;28(11):1963–1972.
27. Young RJ, Gupta A, Shah AD, et al. Potential utility of conventional MRI signs in diagnosing pseudoprogression in glioblastoma. *Neurology*. 2011;76(22):1918–1924.
28. Hu LS, Baxter LC, Smith KA, et al. Relative cerebral blood volume values to differentiate high-grade glioma recurrence from posttreatment radiation effect: direct correlation between image-guided tissue histopathology and localized dynamic susceptibility-weighted contrast-enhanced perfusion MR imaging measurements. *AJNR Am J Neuroradiol*. 2009;30(3): 552–558.
29. Ericson K, Kihlstrom L, Mogard J, et al. Positron emission tomography using 18F-fluorodeoxyglucose in patients with stereotactically irradiated brain metastases. *Stereotact Funct Neurosurg*. 1996;66(suppl 1):214–224.
30. Hatzoglou V, Ulaner GA, Zhang Z, et al. Comparison of the effectiveness of MRI perfusion and fluorine-18 FDG PET-CT for differentiating radiation injury from viable brain tumor: a preliminary retrospective analysis with pathologic correlation in all patients. *Clin Imaging*. 2013;37(3):451–457.
31. Law M. Advanced imaging techniques in brain tumors. *Cancer Imaging*. 2009;9(Special issue A):S4–S9.
32. Law M, Young R, Babb J, et al. Comparing perfusion metrics obtained from a single compartment versus pharmacokinetic modeling methods using dynamic susceptibility contrast-enhanced perfusion MR imaging with glioma grade. *AJNR Am J Neuroradiol*. 2006;27(9):1975–1982.
33. Mitsuya K, Nakasu Y, Horiguchi S, et al. Perfusion weighted magnetic resonance imaging to distinguish the recurrence of metastatic brain tumors from radiation necrosis after stereotactic radiosurgery. *J Neurooncol*. 2010;99(1):81–88.
34. Yun TJ, Park CK, Kim TM, et al. Glioblastoma treated with concurrent radiation therapy and temozolomide chemotherapy: differentiation of true progression from pseudoprogression with quantitative dynamic contrast-enhanced MR imaging. *Radiology*. 2015;274(3):830–840.
35. Choi HS, Kim AH, Ahn SS, et al. Glioma grading capability: comparisons among parameters from dynamic contrast-enhanced MRI and ADC value on DWI. *Korean J Radiol*. 2013;14(3):487–492.
36. Alcaide-Leon P, Pareto D, Martinez-Saez E, et al. Pixel-by-pixel comparison of volume transfer constant and estimates of cerebral blood volume from dynamic contrast-enhanced and dynamic susceptibility contrast-enhanced MR imaging in high-grade gliomas. *AJNR Am J Neuroradiol*. 2015;36(5):871–876.
37. Cha S, Yang L, Johnson G, et al. Comparison of microvascular permeability measurements, K(trans), determined with conventional steady-state T1-weighted and first-pass T2*-weighted MR imaging methods in gliomas and meningiomas. *AJNR Am J Neuroradiol*. 2006;27(2):409–417.
38. Kim YH, Oh SW, Lim YJ, et al. Differentiating radiation necrosis from tumor recurrence in high-grade gliomas: assessing the efficacy of 18F-FDG PET, 11C-methionine PET and perfusion MRI. *Clin Neurol Neurosurg*. 2010;112(9):758–765.
39. Cha S, Lupo JM, Chen MH, et al. Differentiation of glioblastoma multiforme and single brain metastasis by peak height and percentage of signal intensity recovery derived from dynamic susceptibility-weighted contrast-enhanced perfusion MR imaging. *AJNR Am J Neuroradiol*. 2007;28(6):1078–1084.
40. Mangla R, Kolar B, Zhu T, et al. Percentage signal recovery derived from MR dynamic susceptibility contrast imaging Is useful to differentiate common enhancing malignant lesions of the brain. *Am J Neuroradiol*. 2011;32(6):1004–1010.
41. Gupta RK, Awasthi R, Garg RK, et al. T1-weighted dynamic contrast-enhanced MR evaluation of different stages of neurocysticercosis and its relationship with serum MMP-9 expression. *AJNR Am J Neuroradiol*. 2013;34(5):997–1003.
42. Alcaide-Leon P, Rovira A. Dynamic contrast-enhanced MR: importance of reaching the washout phase. *AJNR Am J Neuroradiol*. 2013;34(5):E58–E59.
43. Rathore RK, Gupta RK. Dynamic contrast-enhanced MR: importance of reaching the washout phase. *AJNR Am J Neuroradiol*. 2013;34(5):E60.